# Inter-ELM Power Decay Length for JET and ASDEX Upgrade: Measurement and Comparison with Heuristic Drift-Based Model

T. Eich, B. Sieglin, A. Scarabosio, W. Fundamenski, R. J. Goldston, and A. Herrmann

(ASDEX Upgrade Team)

Phys. Rev. Lett. **107**, 215001 — Published 14 November 2011

DOI: 10.1103/PhysRevLett.107.215001

# Inter-ELM power decay length for JET and ASDEX Upgrade: measurement and comparison with heuristic drift-based model

T.Eich, B.Sieglin, A.Scarabosio, W.Fundamenski[1], R.J.Goldston[2], A.Herrmann,
the ASDEX Upgrade Team and JET-EFDA contributors[3,*]
*Max-Planck-Institut für Plasmaphysik, EURATOM Association, Boltzmannstr 2., D-85748 Garching, Germany*
[1] *EURATOM/CCFE Association, Culham Science Centre, Abingdon, Oxon, OX14 3DB, UK*
[2] *Princeton Plasma Physics Labarotory, Princeton NJ 08543, USA*
[3] *JET-EFDA, Culham Science Centre, Culham, OX14 3DB, UK*
[*] *See the Appendix of F. Romanelli et al., Fusion Energy 2010 (Proc. 23rd IAEA Int. Conf. Daejeon, 2010) IAEA (2010)*
(Received: )

Abstract: Experimental measurements of the SOL power decay length ($\lambda_q$) estimated from analysis of fully attached divertor heat load profiles from two tokamaks, JET and ASDEX Upgrade, are presented. Data was measured by means of infrared thermography. An empirical scaling reveals parametric dependency $\lambda_q/\mathrm{mm} = 0.73 \cdot B_T^{-0.78} q_{cyl}^{1.2} P_{SOL}^{0.1} R_{geo}^{0}$. A comparison of these measurements to a heuristic particle drift-based model shows satisfactory agreement in both absolute magnitude and scaling. Extrapolation to ITER gives $\lambda_q \simeq 1$ mm.

## I. INTRODUCTION

Operation in diverted high confinement mode (H-Mode [1]) is the foreseen scenario for next step tokamak fusion devices. H-mode plasmas develop an edge transport barrier close to the magnetic boundary separating the closed-field-line region from the open-field-line region or scrape-off-layer (SOL). Operation in H-mode is accompanied by periodic relaxation phenomena called edge-localised-modes (ELMs) [2]. The power decay length, $\lambda_q$, in the SOL region is a crucial quantity concerning the divertor peak heat load ($q_{max}$) for current and future devices. Despite the importance of an accurate prediction of $\lambda_q$, a commonly accepted theoretical model or empirical extrapolations from current devices to ITER remain elusive. Such an attempt must include at least two devices with different linear dimensions to establish a major radius dependency, as done in this work where data from ASDEX Upgrade (AUG) and JET are used.

Infrared camera systems with a target resolution of 1.7 mm and framing rates of about 10 kHz are employed. Energy effluxes due to ELMs [3] are observed to impose toroidally asymmetric heat flux ($q$) patterns on the divertor target [4–6] and larger power decay lengths [7]. Additionally as shown in Fig.1, radial movements of the strike line on target, with amplitudes reaching up to the power decay length itself, are observed in JET plasma discharges modulated by ELM induced energy and particle losses [8]. The same phenomenology is observed in AUG. Taking both effects together, ELM averaged estimates of $\lambda_q$ give too large absolute numbers and different parameter dependency [9]. Thus, to reach improved accuracy, inter-ELM periods from 90% to 99% of the ELM cycle time are defined, removing any influences from the latter effects. The heat flux between ELMs and that during ELMs are due to different physical processes. Only by examining them separately can the processes be understood and scaled to future devices. This paper analyses the inter-ELM heat fluxes.

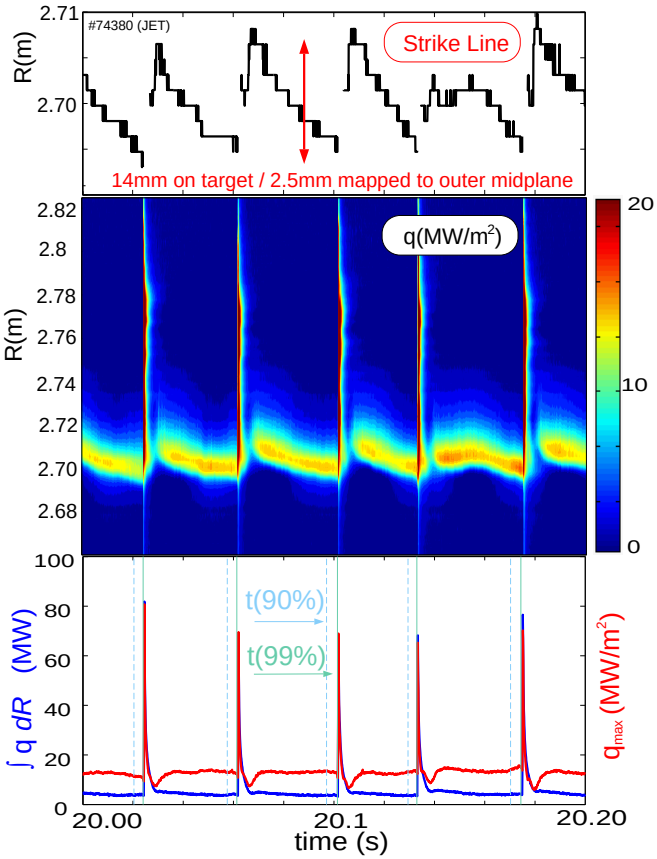


FIG. 1. Evolution of heat flux and the inferred strike line position on the divertor target for a typical JET discharge.

The data base covers 56 and 11 deuterium type-I ELMy H-Mode plasmas for JET and AUG, respectively, summarised in Table I. We denote plasma current as $I_p$, toroidal magnetic field as $B_T$, edge safety factor as $q_{95}$, heating power as $P_h$, averaged triangularity as

$\delta$, effective charge as $Z_{eff}$ and Greenwald density fraction as $n_{GW}$. The aspect ratio of both machines, defined as $\epsilon = a/R_{geo}$, is $\epsilon = 0.32$, with the major geometrical radius denoted as $R_{geo}$ and the minor radius as $a$. The plasma elongation amounts to $\kappa = 1.8$ for both devices. Heat flux profiles are analysed with minimal gas puffing and in the absence of power detachment with carbon divertor plasma-facing components.

TABLE I. Data base of analysed discharges

| | $I_p$[MA] | $B_T$[T] | $q_{95}$ | $P_h$[MW] | $\delta$ | $Z_{eff}$ | $n_{GW}$ |
|---|---|---|---|---|---|---|---|
| JET | 1.0-3.5 | 1.1-3.2 | 2.6-5.5 | 5-24 | 0.2-0.4 | 1.5-2.5 | 0.4-0.8 |
| AUG | 0.8-0.9 | 2.0-2.4 | 4.5-5.1 | 3-13 | 0.2-0.4 | 2.0-2.7 | 0.5-0.7 |

## II. EXPERIMENTAL ESTIMATION OF THE POWER DECAY LENGTH

The SOL power decay length is determined by analysis of heat flux profiles measured on the outer divertor target by means of infrared thermography. Details of the experimental setup for JET can be found in Ref. [7] and for AUG in Ref. [10]. In order to relate the surface heat flux profile to the outer midplane separatrix region, the magnetic flux expansion, $f_x$, has to be taken into account. We use the definition for an integral flux expansion along the target surface [10,11] calculated for the outer midplane region $R = R_{sep}$ to $R = R_{sep} + 5\,\mathrm{mm}$, with $R_{sep}$ being the outer separatrix radius. The variation of $f_x$ by using $R = R_{sep} + 2.5\,\mathrm{mm}$ amounts to <5%.

By expressing the target coordinate as $s$ and the strike line position on target as $s_0$ we describe the heat load profile at the divertor entrance as

$$q(\bar{s}) = q_0 \cdot \exp\left(-\frac{\bar{s}}{\lambda_q f_x}\right) \text{ and } \bar{s} = s - s_0\ ,\ s \geq s_0 \quad (1)$$

This simple ansatz allows to account for perpendicular heat diffusion or *leakage* into the private-flux-region (PFR) by introducing a Gaussian width $S$ representing the competition between parallel and perpendicular heat transport in the divertor volume. This means that, physically, the exponential profile at the divertor entrance [12], is diffused into the private flux region while travelling towards the target [13]. This competition is approximated by a convolution of the exponential profile with a gaussian function with the width $S$ [14]. The target heat flux profiles are thus expressed as ($s \in [-\infty, \infty]$)

$$q(\bar{s}) = \frac{q_0}{2}\exp\left(\left(\frac{S}{2\lambda_q f_x}\right)^2 - \frac{\bar{s}}{\lambda_q f_x}\right) \cdot \mathrm{erfc}\left(\frac{S}{2\lambda_q f_x} - \frac{\bar{s}}{S}\right) + q_{BG} \quad (2)$$

Figure 2 shows examples for measured heat flux profiles and fitting results by using Eq.2 with the free constant parameters $S, \lambda_q, q_0, q_{BG}$ and $s_0$. Two-dimensional numerical heat diffusion calculations [15] using Spitzer-like ($\propto T^{5/2}$) parallel and Bohm-like perpendicular ($\propto T$) thermal diffusivities show that this technique is accurate to better than 6.5% in determining $\lambda_q$ at the divertor entrance in cases where the deduced Gaussian width ($S$) is less than 70% of the exponential width, which is the case for the complete data base. For the mean value of all presented data we get $S/\lambda_q = 0.42$ corresponding to 2% accuracy. Typical values of the field line target inclination angle at $\bar{s} = 0$ are in JET $\simeq 3°$ and in AUG $\simeq 4°$ and relative changes from $\bar{s} = 0$ to $\bar{s} = \lambda_q \cdot f_x$ are between 2% and 14% for both devices.

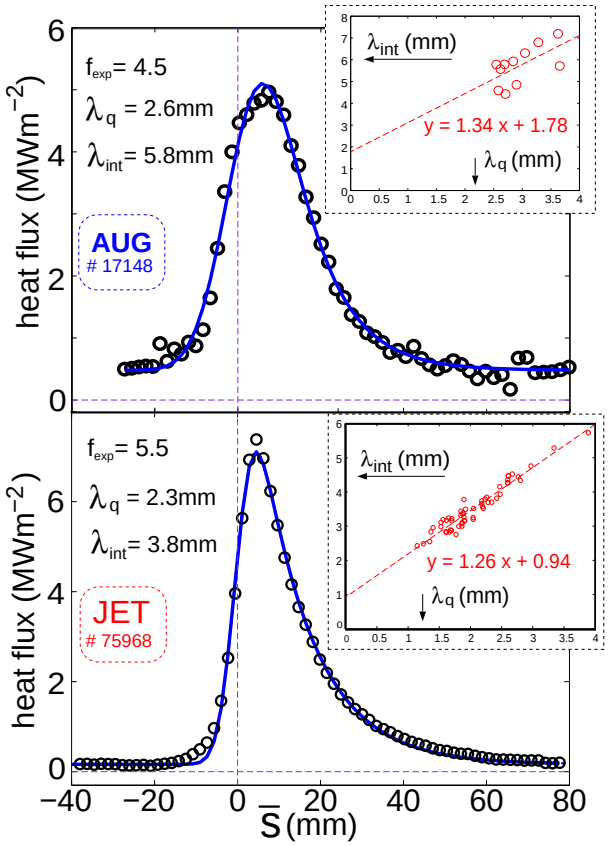


FIG. 2. Heat flux profiles measured on the outer divertor target and fits using Eq.2. The inserts show the relation between $\lambda_q$ and $\lambda_{int}$ which are well expressed by a linear fit.

From Eq.2 follows the integral power decay width [11]

$$\lambda_{int} = \frac{\int (q(s) - q_{BG})ds}{q_{max}} \cdot f_x^{-1} \quad (3)$$

This quantity is frequently used in the literature [11] since it allows to relate the peak heat load on the divertor target to power deposited on the divertor target, a crucial design parameter for the power handling capabilities of a large device such as ITER. The relation between exponential and integral decay lengths for JET and AUG is found by linear least squares fitting to be

$$\lambda_{int}^{JET} = 1.26 \cdot \lambda_q^{JET} + (0.94 \pm 0.32)\,\mathrm{mm} \quad (4)$$
$$\lambda_{int}^{AUG} = 1.34 \cdot \lambda_q^{AUG} + (1.78 \pm 0.68)\,\mathrm{mm}$$

revealing that $\lambda_q$ is not a constant fraction of $\lambda_{int}$ as assumed in earlier studies using simple exponential fit of the SOL part of the heat flux profile [11]. The resulting $\lambda_{int}$ from Eq.2 can be viewed as due to the combination of an exponential profile or parallel heat flux near the plasma, with further radial diffusion both into the PFR and SOL on the divertor side of the x-point. This latter is expected to vary with the divertor geometry, and so would not necessarily be well parametrized by global plasma parameters.

## III. MULTI PARAMETER REGRESSION

We provide here empirical regressions for $\lambda_q$ for JET and for the combined data set from JET and AUG deuterium discharges. A regression for AUG only is not attempted, due to the small variations in $I_p$ and $B_T$. The regression parameters are $B_T$, cylindrical safety factor ($q_{cyl}$), power crossing the separatrix ($P_{SOL}$) and $R_{geo}$ when regressing combined data from both devices. The cylindrical safety factor is expressed by

$$q_{cyl} = \frac{2\pi a \cdot \epsilon \cdot B_T}{\mu_0 \cdot I_p} \cdot \frac{(1+\kappa^2)}{2} \quad (5)$$

The aspect ratio and elongation of both devices are identical and hence cannot be regressed. We apply least square fitting to derive a parametric dependency

$$\lambda(\mathrm{mm}) = C_0 \cdot B_T^{C_B}(\mathrm{T}) \cdot q_{cyl}^{C_q} \cdot P_{SOL}^{C_P}(\mathrm{MW}) \cdot R^{C_R}(\mathrm{m}) \quad (6)$$

Results are summarised in Table II for $\lambda_q$ and $\lambda_{int}$ including the regression variances for each variable. For completeness we note that regressions with $q_{95}$ and $q_{cyl}$ give identical dependencies within the error bars.

TABLE II. Parameter dependency of $\lambda_q$ and $\lambda_{int}$

| | | | $C_0$ | $C_B$ | $C_q$ | $C_P$ | $C_R$ |
|---|---|---|---|---|---|---|---|
| JET | $\lambda_q$ | | 0.70 | -0.84 | 1.23 | 0.14 | - |
| | | $\pm$ | 0.26 | 0.26 | 0.26 | 0.14 | - |
| JET+ | $\lambda_q$ | | 0.73 | -0.78 | 1.20 | 0.10 | 0.02 |
| AUG | | $\pm$ | 0.38 | 0.25 | 0.27 | 0.11 | 0.20 |
| JET | $\lambda_{int}$ | | 1.49 | -0.66 | 0.93 | 0.13 | - |
| | | $\pm$ | 0.43 | 0.19 | 0.19 | 0.11 | - |
| JET+ | $\lambda_{int}$ | | 3.19 | -0.47 | 0.82 | -0.05 | -0.39 |
| AUG | | $\pm$ | 1.49 | 0.21 | 0.25 | 0.09 | 0.18 |

Here we point on the main finding that $\lambda_q$ has a strong dependency on $B_T$ and $q_{cyl}$, minor dependency on $P_{SOL}$. Notably no dependency of $\lambda_q$ on $R_{geo}$ is detected.

## IV. COMPARISON TO HEURISTIC DRIFT-BASED MODEL

Recently a heuristic model has been introduced [16], predicting the absolute value and scaling of the power scrape-off width in H-mode tokamak plasmas. Favourable qualitative comparison with results from a number of experiments was shown. Here we provide a more stringent test of this model against the data base developed from JET and AUG. The model assumes that parallel plasma flow velocity amounts to $c_s/2$ with $c_s$ being the ion sound speed. This sets the particle residence time in the scrape-off layer. The scrape-off layer width is found by multiplying this residence time with the grad B and curvature electron drift velocity. The edge temperature, which determines the drift speed, is found by balancing Spitzer parallel thermal conduction along field lines with the heat flux across the field line. The resulting power fall-off length is given by

$$\lambda_m = 2.02 \cdot \frac{f_{AZ}}{\sqrt{(1+\kappa^2)} \cdot \epsilon^{1/8}} \cdot B_T^{-7/8} \cdot q_{cyl}^{9/8} \cdot P_{SOL}^{1/8} \quad (7)$$

with $\lambda_m$ in [mm], $P_{SOL}$ in [MW], $B_T$ in [T] and

$$f_{AZ} = \left(\frac{2\bar{A}}{1+\bar{Z}}\right)^{7/16} \cdot \left(\frac{Z_{eff}+4}{5}\right)^{1/8} \quad (8)$$
$$\bar{Z} = \sum_i Z_i n_i / \sum_i n_i \;,\; \bar{A} = \sum_i n_i A_i / \sum_i n_i$$

The values for $\bar{A}$ and $\bar{Z}$ are calculated by assuming carbon to be the dominant impurity. The charge state distribution of carbon is taken from Ref. [17] by assuming 100 eV for the separatrix temperature [18].

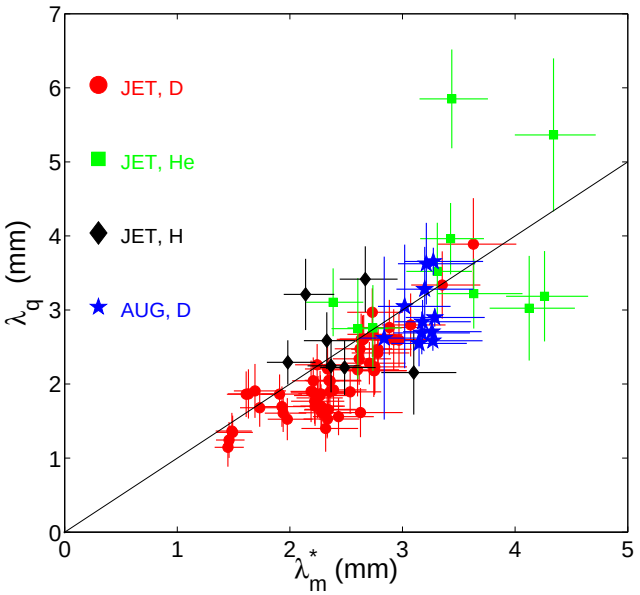


FIG. 3. Comparison of predicted $\lambda_m^*$ to experimental $\lambda_q$ for deuterium (D), hydrogen (H), helium (He) plasmas.

The drift-based model result shown in Eq. 7 represents the mean width of the power scrape-off width poloidally around the plasma, which follows the poloidal flux. Since the JET and AUG results are mapped to the outer midplane, it is appropriate to map $\lambda_m$ to the outer midplane

$$\lambda_m^* = \frac{R_{geo}}{(R_{geo}+a)} \cdot \frac{B_p}{B_p^{mp}} \cdot \lambda_m \text{ with} \quad (9)$$

$$B_p = \frac{\mu_0 \cdot I_p}{2\pi a \cdot \sqrt{(1+\kappa^2)/2)}} \quad (10)$$

and where $B_p^{mp}$ describes the poloidal magnetic field at the outer midplane region. For the data base we find in average $\lambda_m^* = (0.55 \pm 0.05) \cdot \lambda_m$.

Figure 3 shows the comparison of experimental data with the model prediction, complemented by adding 10 helium and 7 hydrogen discharges for JET. Error bars are due to uncertainties in $P_{SOL}$, $Z_{eff}$, carbon charge distribution [17], plasma purity, and experimental estimation of $\lambda_q$. To compare the model prediction to the regression results for deuterium discharges from JET and AUG we use $Z_{eff} = 2$, $\kappa = 1.8$, $\epsilon = 0.32$. As shown in Table III, agreement with both absolute magnitude and scaling dependency is found.

TABLE III. Summary of regression and model prediction

| | $C_0$ | $C_B$ | $C_q$ | $C_P$ | $C_R$ |
|---|---|---|---|---|---|
| $\lambda_m^*$ | 0.92 | -0.875 | 1.125 | 0.125 | 0 |
| $\lambda_q$ | 0.73±0.38 | -0.78±0.25 | 1.20±0.27 | 0.10±0.11 | 0.02±0.20 |

## V. CONCLUSIONS

An approximative expression for the target heat load profiles is introduced. From this expression we are enabled to derive $\lambda_q$ in addition to $\lambda_{int}$. A most notable conclusion of the analysis of $\lambda_q$ is that no machine size scaling is detected which has important impact on future larger machines. As shown in Figure 3, typical numbers for $\lambda_q$ in JET are smaller than in AUG mainly due to the higher $q_{95}$ (or $q_{cyl}$). Given the similar $q_{95}$ (or $q_{cyl}$) value and higher toroidal magnetic field in next step devices such as ITER, smaller values for $\lambda_q$ have to be expected for non detached divertor plasma conditions, when compared with JET. The design values for ITER of interest here are $R$=6.2 m, $a$=2.0 m, $\kappa$=1.7, $P_{SOL}$=120 MW, $B_{tor}$=5.3 T, $I_p$=15 MA, $q_{cyl}$=2.42, $Z_{eff}$=1.6. Extrapolation and model predict for deuterium plasmas $\lambda_q^{ITER}$=0.94 mm and $\lambda_q^{ITER}$=0.97 mm, respectively.

Extrapolation of $\lambda_{int}$ to ITER cannot be given from this work. Assuming that the offset (which is related to the $S$ parameter) between $\lambda_q$ and $\lambda_{int}$ in ITER is similar to JET and AUG, we find for ITER $\lambda_{int} = 1.3 \cdot \lambda_q + (1.36 \pm 0.43\text{mm}) \simeq 2.6 \pm 0.4\text{mm}$. The latter value is close to the lower range of the values predicted in Ref. [19]. However employing a direct extrapolation to ITER from the scaling in table II we find $\lambda_{int} \simeq 1.2$ mm. This is a direct result of the negative size dependence of $\lambda_{int}$ caused by different offsets observed in Eq.4 which are in turn due to the variations of the divertor geometry. The long, baffled divertor in the ITER design may result in larger values of $S$ than observed on AUG or JET. Only dedicated experiments aiming to find a scaling of $S$, can lead to a better understanding here.

The comparison of JET and AUG power fall-off length ($\lambda_q$) for deuterium type-I ELMy H-Modes to the heuristic model prediction [16] of the power scrape-off width, based on parallel convection and curvature drifts, is satisfactory with regard to both magnitude and scaling, and may provide a reasonable baseline for the experimental study of techniques to increase this width.

ITER is anticipated to operate in conditions with a high fraction of SOL radiation and partially detached divertor plasmas, unlike the conditions studied here, but the current assumption [20] that $\lambda_q$ will be in the range of 5 mm, when attached conditions are encountered, needs to be revisited.

## ACKNOWLEDGEMENTS

This work was supported by EURATOM and carried out within the framework of the European Fusion Development Agreement. The views and opinions expressed herein do not necessarily reflect those of the European Commission. This work was supported in part by U.S. DOE under Contract No. DEAC02-09CH11.

[1] F. Wagner *et al.*, Phys. Rev. Lett. **49**, 1408 (1982).
[2] D. Hill *et al.*, J.Nucl.Mater. **241-243**, 182 (1997).
[3] A. Loarte *et al.*, J.Nucl.Mater. **313-316**, 962 (2003).
[4] T. Eich, A.Herrmann, J.Neuhauser, Phys.Rev.Letter **91**, 195003 (2003).
[5] S. Devaux *et al.*, doi:10.1016/j.jnucmat.2011.01.050 .
[6] A. Wingen, T.E.Evans, C.J.Lasnier, K.H.Spatschek, Phys.Rev.Letter **104**, 175001 (2010).
[7] T. Eich *et al.*, doi:10.1016/j.jnucmat.2010.11.079 .
[8] E. Solano *et al.*, Nuclear Fusion **48**, 065005 (2008).
[9] W. Fundamenski *et al.*, Nuclear Fusion **45**, 950 (2005).
[10] A. Herrmann *et al.*, Plas.Phys.Contr.Fus. **44**, 883 (2002).
[11] A. Loarte *et al.*, J.Nucl.Mater. **266-269**, 587 (1999).
[12] P. Stangeby *et al.*, Nuclear Fusion **50**, 125003 (2010).
[13] A. Loarte *et al.*, Contrib. Plasma Phys. **32**, 468 (1992).
[14] F. Wagner, Nucl. Fusion **25**, 525 (1985).
[15] R. Goldston, Physics of Plasmas **17**, 012503 (2010).
[16] R. Goldston, P1.074, 38th EPS Conference on Controlled Fusion and Plasma Physics (2011).

[17] T. Pütterich *et al.*, doi:10.1016/ j.jnucmat.2010.09.052 .
[18] A. Kallenbach *et al.*, Plas.Phys.Con.Fus. **46**, 431 (2004).
[19] W. Fundamenski *et al.*, Nucl.Fusion **51**, 083028 (2011).
[20] ITER Phys. Exp. Group, Nucl.Fusion **47**, S203 (2007).